IEEE Access
Multidisciplinary | Rapid Review | Open Access Journal

Received 9 September 2022, accepted 5 October 2022, date of publication 17 October 2022, date of current version 28 October 2022.

Digital Object Identifier 10.1109/ACCESS.2022.3215270

RESEARCH ARTICLE

Power Scheduling Method for Grid Integration of a PV-BESS CHB Inverter With SOC Balancing Capability

DIEGO IANNUZZI, MARINO COPPOLA, PIERLUIGI GUERRIERO, (Member, IEEE), ADOLFO DANNIER, (Member, IEEE), AND ANDREA DEL PIZZO, (Member, IEEE)
Department of Electrical Engineering and Information Technology, University of Napoli Federico II, 80125 Naples, Italy
Corresponding author: Adolfo Dannier (adolfo.dannier@unina.it)

ABSTRACT The paper deals with a single-phase photovoltaic (PV) inverter based on the Cascaded H-Bridge (CHB) topology for Low Voltage (LV) grid. A distributed architecture of PV sources integrated with battery energy storage systems (BESS) is proposed with the particularity of avoiding the use of dc-dc converters. A method of compensating for the short-term daily variability of PV energy is also presented. The control implements power scheduling to ensure that constant active power is fed into the grid at every predetermined time interval (e.g., every quarter of an hour). Furthermore, a dedicated hybrid modulation scheme based on a sorting algorithm for balancing the state of charge (SOC) of the single cells is proposed. Numerical investigations are carried out on a 19-level CHB inverter implemented in a PLECS®(i.e., the simulation platform for power electronic systems from Plexim) environment to validate the feasibility and effectiveness of the proposed control strategy.

INDEX TERMS Battery integration, hybrid modulation, power scheduling, PV-CHB inverter, short-term variability, variable renewable energy.

I. INTRODUCTION

The ongoing energy transition from fossil to zero carbon sources requires an ever-increasing sharing of Variable Renewable Energy sources (VRE) [1], whose management will play a central role in increasing the flexibility of the in future power distribution networks. The grid integration of VRE sources becomes essential and must ensure a high quality, reliable and uninterrupted power supply. In this perspective, each national Distribution System Operator (DSO) establishes a regulatory framework (Grid Code) to guarantee the transmission and dispatching of energy and the security of the grid. Furthermore, precise and stringent rules are defined for the integration of renewable energy sources, also with reference to power quality.

The associate editor coordinating the review of this manuscript and approving it for publication was Akshay Kumar Saha.

The problem of intermittency of PhotoVoltaic (PV) generation can be solved through the use of different types of energy storage technologies. In recent years, various topologies of converters with integrated batteries [2], [3], [4], [5] have been proposed to attenuate fluctuations in PV power and, at the same time, to ensure acceptable values of harmonic distortion factors of the currents.

The solutions proposed in the literature are usually classified into two different categories:

- a centralized BESS which allows to exploit the energy produced during the hours of sunshine for the rest of the day. It is sized to store the average energy produced in the daytime by the PV sources and is connected to the dc-link (dc side) of a typical dual-stage inverter or directly to the ac output (ac side) [6], [7], [8], [9], [10];
- a distributed BESS which acts as a dynamic energy buffer to compensate for mismatch among modules (e.g., due to partial shading) and fluctuation in energy

production (e.g., due to rapidly changing weather conditions), thus allowing the inverter to meet the power demand of the grid with a flat profile of energy production [11], [12], [13], [14].

The latter approach appears to be very promising due to its greater flexibility. The practical implementation can find a suitable solution in multilevel inverters (MLI), in which the energy storage elements can be integrated in a distributed way, with evident advantages in terms of power control and management [15], [16]. When using the MLI topology, the power fluctuation problem can be addressed in two different ways: in some solutions there is full integration of the batteries and the PV panel, i.e., one group for each submodule (i.e., inverter stage) of the MLI [17], [18], [19]; other solutions provide for partial integration, with one or more batteries connected to the dc-link instead of to the PV panel [20], [21], [22] (so-called hybrid system). However, in all cases mentioned, the integration of each battery always requires an interface dc/dc converter capable of managing the charging/discharging phases during operation. This can be an advantage for the control capability, but it determines an undeniable increase in the overall volume, weight, and purchase cost of the converter and in subsequent maintenance costs. Moreover, a reduced efficiency is expected.

The solution proposed in this paper is based on a multilevel Cascaded H-Bridge Inverter (CHB), for which each power cell (i.e., the H-Bridge circuit) is integrated with its own battery storage unit connected directly to the dc-link without any dc/dc converter for the corresponding interfacing. A unidirectional dc/dc converter is used only for the connection of the photovoltaic generator (PVG) to the dc-link. The proposed circuit configuration in PV-BESS CHB inverter represents a novelty with respect to the solutions of [17], [18], [19], [20], [21], [22].

The main objective of the paper is to ensure a constant supply of energy to the grid, even in the absence of dc/dc converters, keeping the SOC of the batteries included in each power cell balanced [23], [24], [25]. In particular, the control technique is based primarily on an appropriate selection of a time window during which the system can supply a predetermined constant power value to the grid. The chosen time interval is 15 minutes, corresponding to the period in which the Italian DSO verifies how much power is required to satisfy the demand.

This is also in accordance with the concept of *Short-Term Variability* (STV), i.e., a variability of PV generation that occurs in a few minutes, thus leading to a different allocation of power during the typical daily cycle on-off of solar radiation. The reference power to be delivered (i.e., the programmed power) considers the average behavior of the PV generation profile and the SOC level of each battery to balance the SOCs of the batteries under different operating conditions. The latter result is achieved by using a suitable hybrid modulation scheme based on a sorting algorithm to decide which power cell of the cascade must be inserted (mode ± 1), bypassed (mode 0) or driven in PWM mode. The proposed modulation technique also allows to include in the Distributed Maximum Power Point Tracking (DMPPT) algorithm a control of the modulation index to operate a power cell in the overmodulation region, thus ensuring the stability of the system even in the case of deep mismatch among the PV modules.

The paper is organized as follows: section II presents the mathematical model of the PV-BESS CHB inverter, while the hierarchical control system is discussed in section III. Section IV show the numerical results for the real case study; finally, conclusions and observations are drawn in section V.

II. MULTILEVEL PV INVERTER WITH INTEGRATED BATTERY

The proposed architecture of distributed PV-BESS based on CHB inverter (Fig. 1) consists of N series-connected power cells each of which comprises a double stage inverter whose dc-link a BESS is directly connected without any converter interface. A filter inductor L connects the CHB output to the grid, enabling the injection of a sinusoidal current with a desired power factor.

In more detail, each PV module is interfaced to dc-link by means of a unidirectional dc/dc boost converter able to transfer the power from the PV source to the dc-link. Its main role is to maximize the solar power extraction from each PVG. At this aim, a DMPPT is implemented, thus performing an independent control of each PV module.

On the other hand, the main task of the inverter (i.e., H-bridge) is the transmission of the desired active power to the grid, while allowing the SOC balancing thanks to a dedicated sorting algorithm used to perform the hybrid modulation strategy.

The converter operation can be described by an averaged modeling approach, so anticipating the choice made to perform suitable and effective simulations by means of averaged switch network.

Each circuit parameter can be expressed as follows:

$$X = \langle x(t) \rangle_{T_s} = \frac{1}{T_s} \int_{t}^{t+T_s} x(\tau) d\tau \tag{1}$$

where T_s represents the switching period of the dc/dc converter, whose duty cycle is

$$d_i = \frac{T_{on,i}}{T_s} \quad i = 1, .., N \tag{2}$$

Low-frequency average of circuit parameters is found by evaluation of (1), thus the following equations describe how the low-frequency components of inductor, capacitor, and BESS of the converter evolve in time (see Fig. 1):

$$\frac{dI_{grid}}{dt} = \frac{\sum_{i=1}^{N} s_i V_{dc,i} - V_{grid}}{L}$$
$$\frac{dV_{dc,i}}{dt} = \frac{I_{out,i} - s_i I_{grid}}{C_{dc,i}}$$

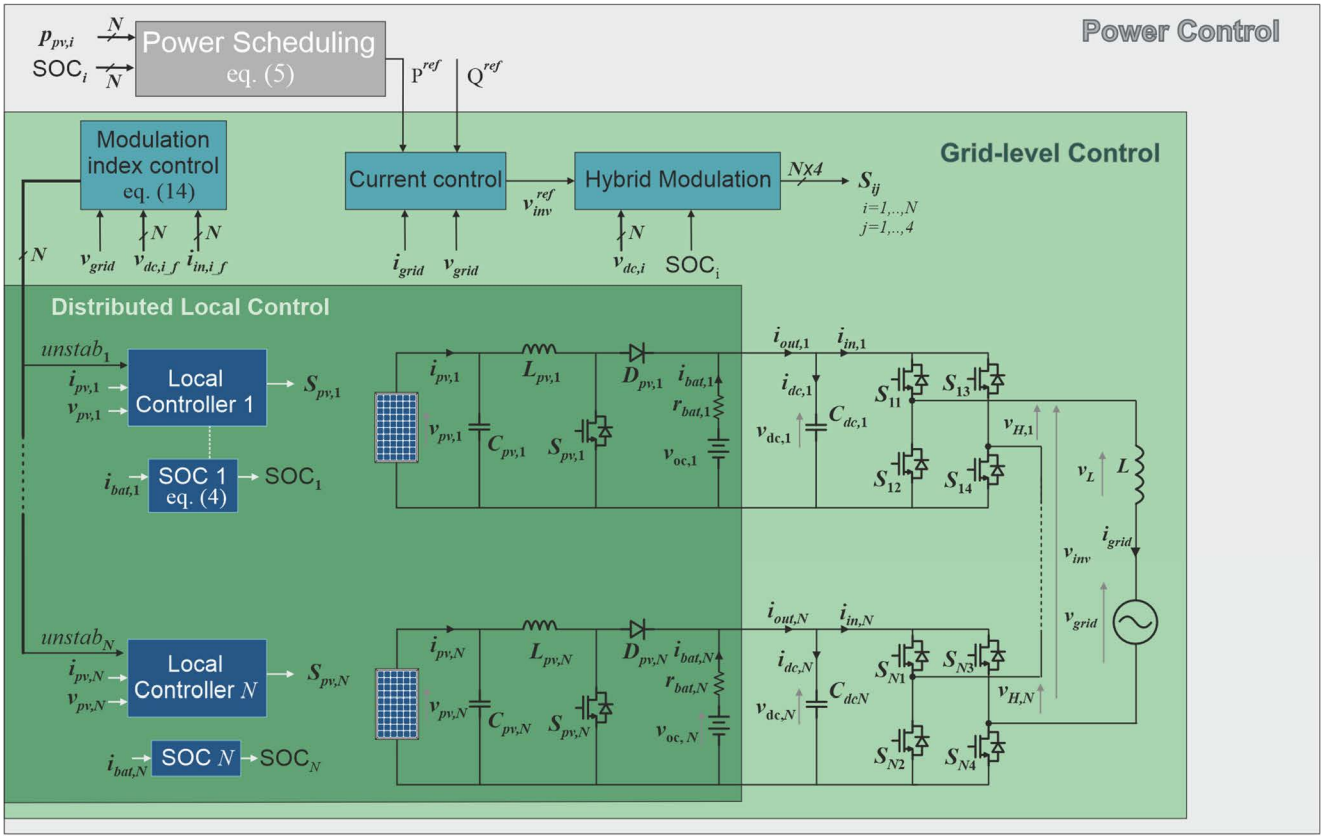

FIGURE 1. Schematic view of $2N + 1$-level double-stage PV CHB inverter along with its control architecture.

$$\frac{dI_{pv,i}}{dt} = \frac{V_{pv,i} - (1 - d_i)V_{dc,i}}{L_{pv,i}}$$
$$I_{out,i} = (1 - d_i)I_{pv,i} \quad i = 1, .., N \tag{3}$$

where s_i is the continuous switching function, which replaces the discrete control signal of each H-bridge, and it can be considered constant during T_s. $V_{dc,i}$, $V_{pv,i}$, and V_{grid} are the mean values of i-th dc-link voltage, i-th PV voltage, and grid voltage, respectively. Moreover, $I_{out,i}$, $I_{pv,i}$, and I_{grid} are the mean values of i-th output current, i-th PV current, and grid current, respectively.

Finally, each power cell is equipped with its own storage unit connected directly to the inverter dc-link, so leading to a distributed battery energy storage system integrated into the multilevel structure. It is worth noting that this connection choice avoids adding one more power converter, thus resulting in weight and cost reduction, while also enhancing overall efficiency and reliability. The battery behavior is modeled by an equivalent circuit made up of an ideal voltage source, which represents the open-circuit voltage v_{oc}, in series with a constant internal resistance r_{bat}. To simplify the model only the v_{oc} dependence on SOC is considered:

$$V_{bat,i} = V_{oc,i}(SOC_i) + r_{bat,i}I_{bat,i}$$
$$I_{bat,i} = -\frac{Q_{bat,i}}{3600}\frac{dSOC_i}{dt} \quad i = 1, .., N \tag{4}$$

where $V_{bat,i}$, $I_{bat,i}$, and $Q_{bat,I}$ are the i-th battery voltage, current and capacity, respectively.

III. HIERARCHICAL CONTROL STRATEGY

The control strategy of the CHB inverter is based on a hierarchized architecture organized on three layers, namely power, grid-level and distributed local control. A detailed description is provided in Fig. 1. The behavior of the three layers of the control can resumed as follows:

Power control – It periodically defines the active power reference to be followed by the grid-level control. In the control period T_{ref} (i.e., 15 minutes), the CHB inverter will supply to the grid a constant active power, P^{ref}, obtained by considering the average PV power production and the SOC levels aiming to balance the SOCs by keeping them close to a desired level.

Grid level - A global current control ensures to inject into the utility grid the desired amount of active and reactive power. A specific hybrid modulation strategy is implemented, also allowing to balance the batteries SOC by means of a suitable sorting algorithm.

Local distributed control - It regulates the power generation for each cell individually. Local controllers implement both the modified MPPT algorithm and the voltage control loop of the dedicated boost converters.

The execution time periods of the main control blocks are reported in the following Table

TABLE 1. Execution time of control blocks.

Time	Value
T_{ref} (min.)	15
T_{MPPT} (ms)	50
T_{fort} (ms)	0.2

It is worth highlighting that each control loop is able to reach the desired steady-state behavior well before the correspondent reference is changed at each execution time interval as confirmed by the simulated results shown in the next section.

A. POWER CONTROL

The power control implements the power scheduling to ensure that a constant active power is injected into the grid in the time interval T_{ref}. The active power reference is defined at the beginning of each interval and kept constant until the end.

The active power reference P^{ref} to be injected into the utility grid during the k-th time interval is calculated as

$$P^{ref}(k) = \sum_{i=1}^{N} \left(P_{pv,\,i}(k) - \Delta SOC_i(k) \cdot P_{pv,\,rated}\right) \tag{5}$$

where the first contribution is estimated as the average PV power produced in the previous time interval

$$P_{pv,\,i}(k) = \frac{1}{T_{ref}} \int_{(k-1)T_{ref}}^{kT_{ref}} V_{pv,\,i}\, I_{pv,\,i} dt \tag{6}$$

because it varies with the weather conditions. Instead, the actual deviation ΔSOC_i w.r.t. the SOC reference value, SOC*, represents the SOC error and it is determined as

$$\Delta SOC_i(k) = SOC^* - SOC_i(k) \tag{7}$$

while $P_{pv,rated}$ represents the rated power of each PV module at standard test conditions (i.e., 331.55 W at 1000 W/m^2, $T_{amb} = 25°C$).

Each of the N cells is supposed to be able to contribute to the overall output active power with its input PV power (i.e., the power supplied by the corresponding PV source) and with the power the battery must provide/absorb during the interval T_{ref} to track the reference value, SOC*.

It should be remarked that, as mentioned above, the sorting algorithm operates a balance action on the batteries SOC. Accordingly, if the PV sources and the battery stacks evenly operate (i.e., $P_{pv,i}(k)$ is the same for each cell as well as $\Delta\text{SOC}_i(k)$), the active power reference P^{ref} can be expressed as

$$P^{ref}(k) = N\left[P_{pv,\,i}(k) - \Delta SOC_i(k) \cdot P_{pv,\,rated}\right] \tag{8}$$

thus, implementing a proportional control on the batteries SOC and keeping them close to the reference value, SOC*, at steady state.

Moreover, to ensure a proper behavior, the battery capacity Q_{bat}, expressed in ampere per hour, is sized as

$$Q_{bat} \approx 3600 \frac{P_{pv,rated} 4T_{ref}}{V_{bat,nom}} \tag{9}$$

to make the batteries able to store the energy producible by the PV source in an hour (i.e., $4T_{ref}$).

B. GRID-LEVEL CONTROL

The grid-level control loop has the main task of controlling the grid current (see Fig. 2) whose control strategy is generally based on the instantaneous power theory (IPT), namely on the $p - q$ theory, which operates with time components voltages, $V_{grid,\alpha\beta}$, and currents$I_{grid,\alpha\beta}$ expressed in the stationary reference frame, $\alpha\beta$. In the proposed single-phase system, the required quantities in the $\alpha\beta$ coordinates are obtained thanks to a second order generalized integrator (SOGI), which represents a well-established method for quadrature signal generation (QSG) [26], [27] The components of grid current reference, $I^{ref}_{grid,\alpha\beta}$, are functions of the desired instantaneous activeP^{ref} and reactive, Q^{ref} powers Thus, they are expressed by:

$$\begin{bmatrix} I^{ref}_{grid,\alpha} \\ I^{ref}_{grid,\beta} \end{bmatrix} = \frac{1}{V^2_{grid,\alpha} + V^2_{grid,\beta}} \begin{bmatrix} V_{grid,\alpha} & V_{grid,\beta} \\ V_{grid,\beta} & -V_{grid,\alpha} \end{bmatrix} \times \begin{bmatrix} P^{ref} \\ Q^{ref} \end{bmatrix} \tag{10}$$

The estimation of phase angle for grid voltage synchronization is carried out by PLL. Then, only the α component is controlled in our single-phase system, thus the power reference, P^{ref}, is determined by the power scheduler at power control level, while the power reference, Q^{ref}, is supposed to be required by the utility grid supervisor, to let the inverter performing ancillary service.

The evaluation of output inverter reference voltage is carried out by the time domain resonant controller [17] [28], [29]. This latter processes the actual feedback grid current error, $\varepsilon^{ref} = I^{ref}_{grid,\alpha} - I_{grid}$ The output of resonant controller is the voltage across the filter inductance, V^{ref}_L, expressed in implicit differential and integral form by:

$$\frac{dV^{ref}_L}{dx} + \omega_0^2 \int_0^t V^{ref}_L dt + \varepsilon^{ref} = 0 \tag{11}$$

Thus, the reference inverter voltage is given by:

$$V^{ref}_{inv} = V^{ref}_L + V_{grid,\,\alpha} \tag{12}$$

1) MODULATION INDEX CONTROL

The power which can be provided by each cell is directly related to the amplitude of its modulation index. The cell which presents the higher power content also shows the higher modulation index whose value can overcome the unity in case of deep mismatch among the PVGs. In fact, this operating condition can lead the most powerful cell in the overmodulation region, theoretically up to a value of modulation

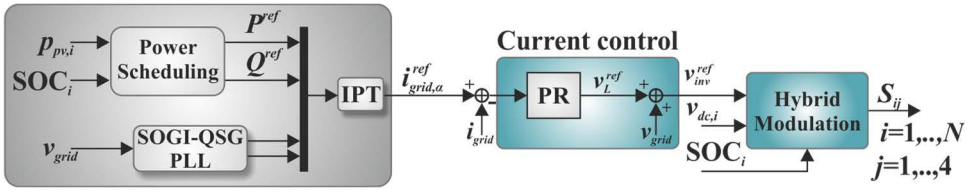

FIGURE 2. Detailed view of the main control loop of the CHB inverter.

index equal to $4/\pi$, which represents the maximum allowable power capability of a cell. The possibility of reaching the full square-wave operation (i.e., $m_i = 4/\pi$) is due to the used modulation strategy. In our case, it is not possible to achieve a full square-wave operation because at least one cell will be in PWM mode at each control step. Nevertheless, the overmodulation region can be exploited with no detrimental effect on the inverter output power quality.

The modulation index control acts by considering the following expression:

$$m_i = \frac{V_{grid,\max}}{\frac{1}{I_{in,i}} \sum_{j=1}^{N} I_{in,j} V_{dc,ave,j}} \tag{13}$$

where $V_{grid,\max}$ is the amplitude of the grid voltage, $V_{dc,ave}$ is the average dc-link voltage. If m_i is greater than the decided upper limit, m_{iUL}, the stability flag (i.e., $unstab_i$) goes high. This latter is one of the inputs of the local controller where the MPPT is performed. When $unstab_i = 1$, the PV voltage reference is increased (i.e., the PV current is reduced), regardless of MPPT decision, until m_i becomes lower of the fixed upper limit. The effectiveness of the modulation index control in obtaining the desired system behavior will be clearly shown in the following.

2) HYBRID MODULATION CONTROL

The modulation control dynamically assigns to the individual cells a specific switching mode (SM_i), namely 1, −1, 0, and PWM.

For sake of simplicity, we can consider the behavior in the positive half-wave of the grid voltage. The basic idea is to hold the cells with larger SOC in 1 mode to favor the discharge, while holding the cells with lower SOC in −1 mode to let them charge. As shown in Fig. 3, according to the hybrid approach, only one cell is switching (i.e., PWM mode).

The modulation strategy, described in the flow-chart in Fig. 4 in the case of positive half-wave inverter voltage, can be resumed in the following steps:

- firstly, the power cells are sorted in ascending order of the SOC_j, where j is index of sorted cells (the ordering index j does not correspond to the physical position of the cells in the cascade indicated by index i). At each element of the sorted vector corresponds the related dc-link voltage, used in the next step;

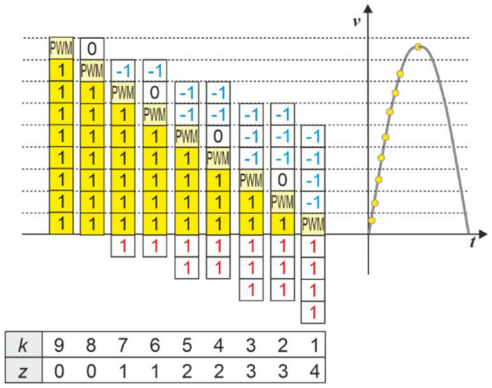

FIGURE 3. Hybrid modulation strategy.

- the minimum number k of cells needed to synthesize the actual voltage reference V_{inv}^{ref} (yellow boxes in Fig. 3) is defined by means of an iterative procedure shown in Fig. 4;
- the Nk remaining cells are supposed to not contribute to the inverter voltage V_{inv}: even though the simplest way is to keep all of them in 0 mode, such a result can be reached also if some cells are kept in −1 mode and then compensated by increasing 1-mode cells by the same number. Thus, the overall contribution will be zero, as desired. According to this, the maximum allowed number z of the upper cells is obtained as

$$z = \frac{N - k - \mathrm{mod}(N - k, 2)}{2} \tag{14}$$

  will be set to -1 mode, while the k-1 lower cells will be kept in 1 mode;
- being defined $k' = k + z$, only the $k'th$ cell will operate in PWM mode with a duty-cycle calculated as

$$d = \frac{V_{inv}^{ref} - \sum_{j=k}^{k+z-1} V_{dc,j}}{V_{dc,k'}} \tag{15}$$

  while the k'-1 lower cells will be kept in 1 mode;
- the remaining cell will set in 0 mode.

C. DISTRIBUTED LOCAL CONTROL

As mentioned earlier, the local controller in Fig. 5 is mainly responsible for the regulation of the power production of each cell individually. In particular, MPPT regulator is employed

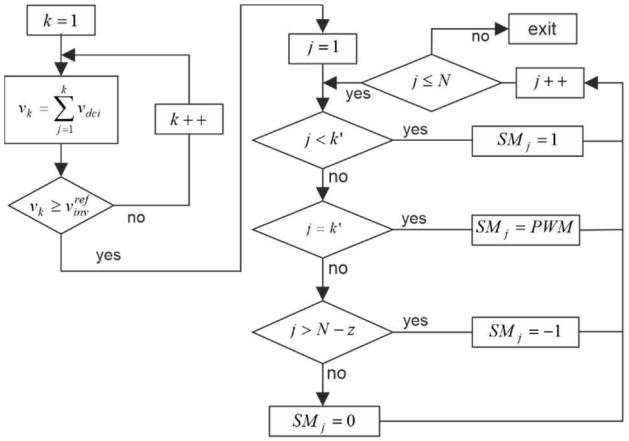

FIGURE 4. Hybrid Modulation flow-chart: case of positive half-wave.

to harvest as much real power as possible by controlling the PV voltage by means of dc/dc boost converter.

1) MPPT AND DC/DC BOOST CONVERTER CONTROL

The proposed DMPPT approach consists in a dedicated MPPT controller for each power cell, which performs individual MPP tracking of each PV module, based on the conventional Perturb&Observe algorithm properly modified accounting for the modulation index control It is worth noting that the used MPPT algorithm does not contain any specific modification enabling the tracking of possible local maxima in the PV characteristic due to partial shading phenomena. In fact, the main issue to be addressed is the power mismatch among the PV modules which is obtained by only considering a uniform shading (i.e., the PV characteristic exhibits a single MPP), thus allowing the conventional P&O algorithm to properly track the MPP.

The positive gradient algorithm is performed on the PV voltage and current, filtered to attenuate the 100 Hz component due to the power injection into the grid. The iteration period is $T_{MPPT} = 50\ ms$

At each iteration, the output voltage reference, $V_{pv,i}^{ref}$ is increased by a constant voltage step $\Delta = 0.3\ V$ in the following cases:

- the input power exhibits a positive gradient;
- the power cell operates with a not allowed modulation index ($unstab_i = 1$);

A voltage control for the boost converter has been implemented. The PV voltage error ε_{pvi}, defined as

$$\varepsilon_{pvi} = V_{pv,i\_f} - V_{pv,i}^{ref} \tag{16}$$

where V_{pvi_f} is the filtered input PV voltage. Then, it is processed by a PI controller to calculate the duty cycle, d_i, to proper control the dc/dc boost converter, so allowing to track the MPP of the corresponding PV module, as reported by:

$$d_i = k_p \varepsilon_{pv,i} + k_i \int_0^t \varepsilon_{pv,i}\, dt \tag{17}$$

IV. SIMULATED PERFORMANCE

A set of simulations has been performed on a 19-level CHB inverter (i.e., $N = 9$) implemented in the PLECS®environment to validate the feasibility and effectiveness of the proposed control strategy. In order to reduce the computational load, and to verify the system dynamics in a reasonable simulation time, the following steps have been taken:

- the average model of power circuits has been used;
- the battery capacity has been properly downscaled in order to show in one second the behavior equivalent to one hour of operation (e.g., $Q_{bat\_equivalent} = Q_{bat} / 3600\ Ah$);
- the used PV profile has also been scaled to meet the previous requirement (i.e., one second corresponding to one hour).

In particular, the used PV profile has been downloaded from the *Photovoltaic Geographical Information System* (PVGIS) [30] and it is depicted in Fig. 6 (red line). It represents the daily average irradiance profile during the month of April in Naples in clear-sky conditions.

Nevertheless, it must be considered that PV generation is inherently intermittent because, although the amount of sunlight reaching the PV modules follows a regular pattern on average, atmospheric changes, presence of obstacles can determine undesired and unpredictable PV power fluctuations. Cloudiness phenomenon can especially result in sudden reduction of PV power which recovers the previous level when the clouds move away from the PVGs.

This event can occur in very short time and the consequent rate of change of PV production is very quick due to lack of inertia in PV systems. Therefore, solar irradiance and the corresponding PV generation can drastically vary in few seconds [2], thus determining relevant PV power changes in relatively short period.

Usually, you can refer to this as STV, which accounts for a PV generation variability over a time interval of 15 minutes. This latter corresponds to the period at which the DSO verifies how much power is needed to meet the consumers demand. Consequently, the PV profile in Fig. 6 (blue line) has been properly modified to introduce a STV. This behavior has been obtained by introducing sudden variations of solar irradiance (i.e., the rise and fall time duration is equal to ten seconds) in each period of a quarter of hour with a 40% reduction of the clear-sky performance.

The operating point at standard test conditions (STC) of the used PV panel is $P_{MPP} = 331.55\ W$ corresponding to $V_{MPP} = 37.6\ V$ and $I_{MPP} = 8.82\ A$, while used BESS shows a capacity of 7.5 Ah, with a rated voltage of 48 V and a total internal resistance of 30 $m\Omega$. The line inductor presents an

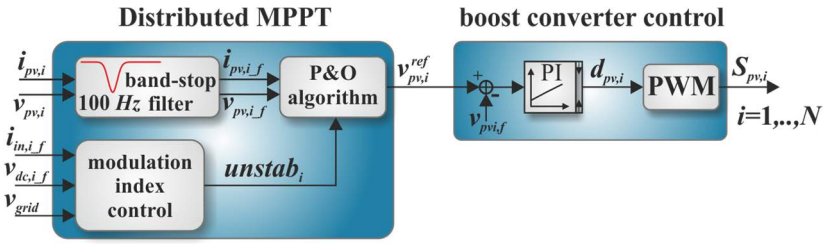

FIGURE 5. Detailed view of local controller.

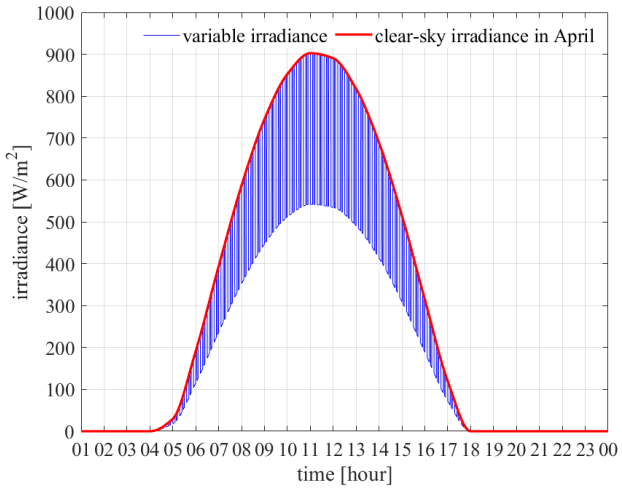

FIGURE 6. Daily average irradiance profile during the month of April in Naples.

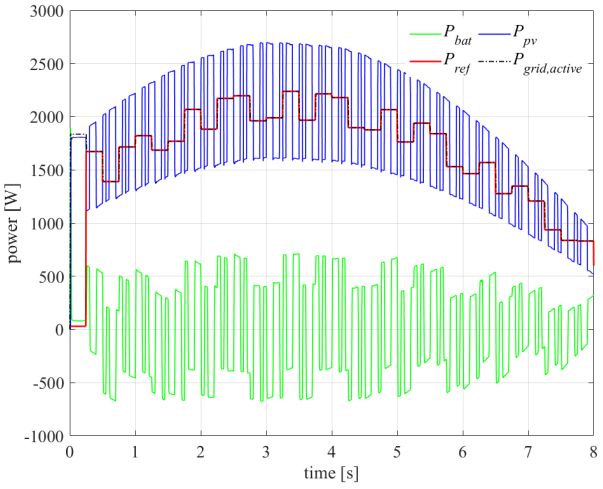

FIGURE 7. Power behavior: PV power (blue line), battery power (green line), reference power (red line), and grid active power (dashed black line).

inductance $L = 10\ mH$. The number of cells making up the multilevel inverter cascade has been initially chosen to assure the active power injection to the grid. For this purpose, the sum of the dc-link voltages of the individual cells must be adequately greater than the peak grid voltage.

In our case, by considering the circuit parameters and the maximum available power, a minimum number of 8 cells should be considered. Nevertheless, the chosen number was 9 to provide a redundancy able to enhance system reliability, fault-tolerance and safety operation. Then, it is worth highlighting that the dc-link voltage of each power cell is greater than the open-circuit voltage of PV module to operate the front-end dc/dc converter in step-up mode.

The performance of the proposed system has been mainly verified in two operating modes: uniform and mismatch dynamic conditions. In particular, it has been considered the daily behavior in a range of eight hours extending from 8:00 AM to 4:00 PM. As mentioned above, the corresponding simulation time spans from 0 to 8 seconds. The obtained results are discussed in the following sub-sections.

A. UNIFORM DYNAMIC CONDITIONS

In such a case, all the PV modules follow the behavior shown in Fig. 6 in the time window 08÷16 (i.e., 8:00 AM÷4:00 PM).

As discussed in the previous sections, the main issue to be addressed is the SOCs balancing. This goal is achieved thanks to the sorting algorithm performed on the SOC error (i.e., SOC* - SOC_i) to identify which battery must be charged (positive error) or discharged (negative error) more than the others. The SOC* is chosen equal to 60% to avoid overcharge or deep discharge meanwhile the batteries can follow the desired behavior (i.e., mitigation of the PV power fluctuations) [25], [31].

Firstly, Fig. 7 shows the power behavior, and it can be easily deduced the effectiveness of the control action. In fact, the reference power P^{ref} (see eq. (8)) tracks on average the PV power whose fluctuations are mitigated by the storage elements, thus, allowing to provide to the grid the scheduled power.

The batteries behavior in terms of SOC is depicted in Fig. 8(a). Initially, it shows an increasing trend, then in the post-meridian part of the day a decreasing one, as expected. The final SOC value of each battery is of about 0.55 (i.e., very close to the desired value of 0.6).

Moreover, to prove the validity of the proposed balancing control, the results obtained from two other simulations have been superimposed to that of Fig. 8(a). In particular, the difference is due to the initial SOC value: in the first case, it is equal to 0.9; in the second one, it is equal to 0.4.

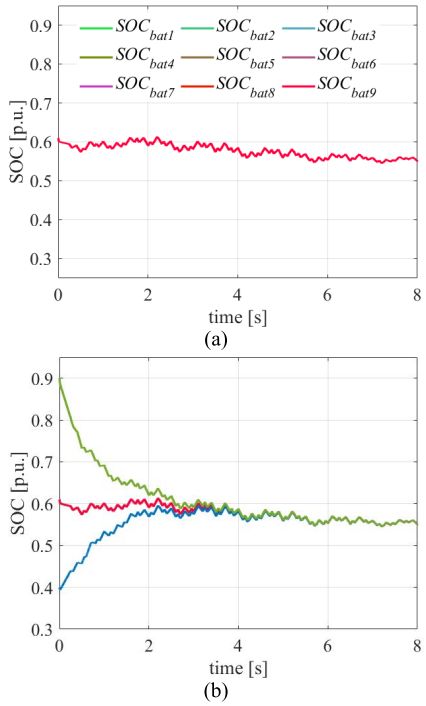

FIGURE 8. (a) SOC versus time of the nine batteries; (b) SOC behavior in three different initial conditions: $SOC_{initial} = 0.9$ (green line); $SOC_{initial} = 0.4$ (blue line); $SOC_{initial} \approx 0.6$ (red line).

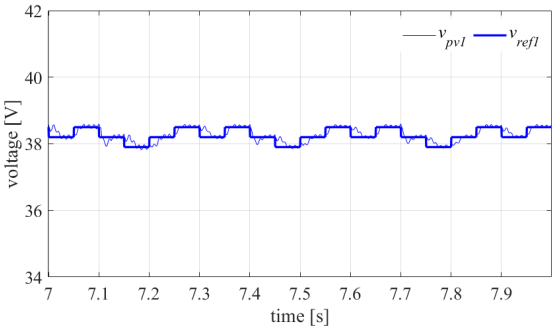

FIGURE 9. MPP tracking behavior of cell#1.

Despite the initial SOC conditions are different, Fig. 8(b) reveals that the implemented control can force each cell to reach the desired behavior in all three cases.

The MPP tracking of the first cell is reported in Fig. 9, as an example. The dc-link voltages are shown in Fig. 10, and as expected in uniform conditions they result well balanced as well as the modulation indexes which assume the nominal value of about 0.75 and no overmodulation occurs (see Fig. 11). Anyway, the upper limit of the modulation indexes is fixed to 1.2, so accounting for the possibility of going to overmodulation region.

The grid behavior (voltage and current) along with the inverter output voltage (modulated voltage) are depicted in Fig. 12. The grid current appears sinusoidal in phase with grid voltage, thus leading to an almost unitary power factor.

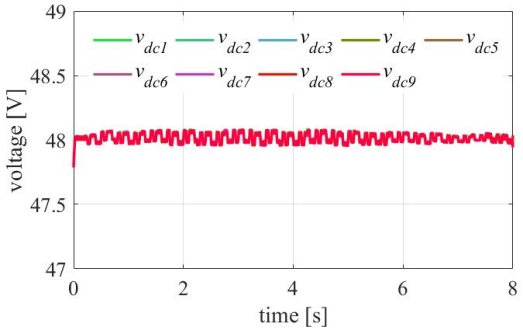

FIGURE 10. Voltage behavior at dc-link.

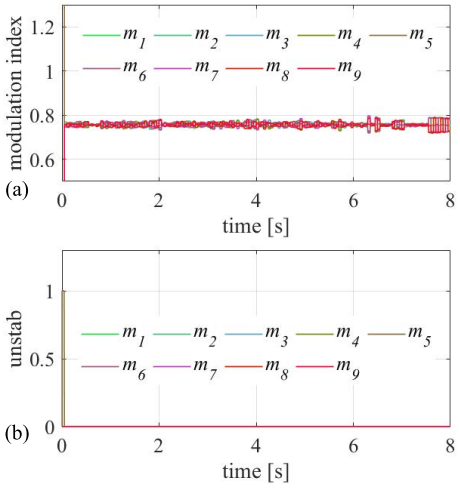

FIGURE 11. Modulation indexes (a), and stability flag (b).

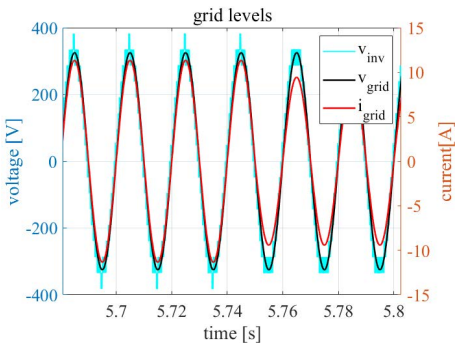

FIGURE 12. Behavior of grid current (red line), modulated voltage (cyan line), and the grid voltage (black line).

B. MISMATCH DYNAMIC CONDITIONS

This simulation considers the effect of mismatch among the PVGs. It has been considered a worst case in which one cell (i.e., the first one in our case – cell#1) shows a behavior like Fig. 6 but with a 20% reduction of the clear-sky performance, while the other N-1 cells with a 60% reduction of the clear-sky performance, as can be inferred from Fig. 13.

The power behavior is shown in Fig. 14. It allows to check the suitable control action which results in an active power

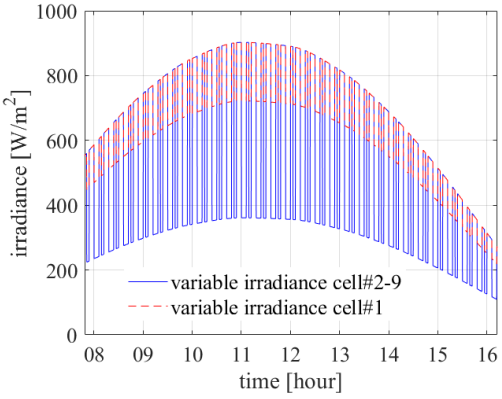

FIGURE 13. Irradiance profile of cell#1 (red dashed line), and of the remaining 8 cells (blue line).

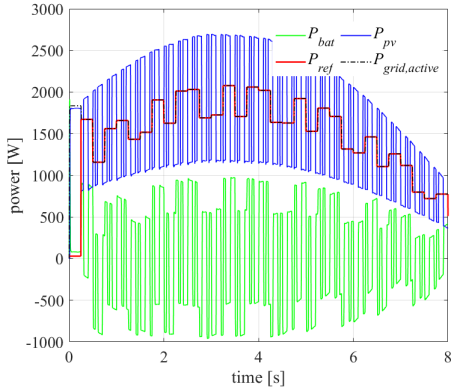

FIGURE 14. Power behavior: PV power (blue line), battery power (green line), reference power (red line), and grid active power (dashed black line).

provided to the grid according to the reference power. Moreover, the SOCs appear to be well balanced as in the uniform case.

The main difference from the uniform case is that to obtain the SOC balancing, the output power of the most powerful cell is no longer balanced with the other cells as can be deduced from Fig. 15, which reports the average output power behavior of the CHB power cells. In average the most powerful cell (i.e., cell#1) must obviously handle its higher power content, which is directly related to the amplitude of its modulation index.

In fact, the cells with higher power operate at higher modulation indexes, while sharing the same output current in the cascade [32].

Moreover, in case of deep mismatch among the PVGs, the modulation index of the most powerful cell can easily reach the overmodulation region.

As aforementioned, in our case the upper limit is fixed to 1.2, while the maximum allowable could be $4/\pi$ (corresponding to the square-wave operation), which represents the maximum theoretical power capability of a cell.

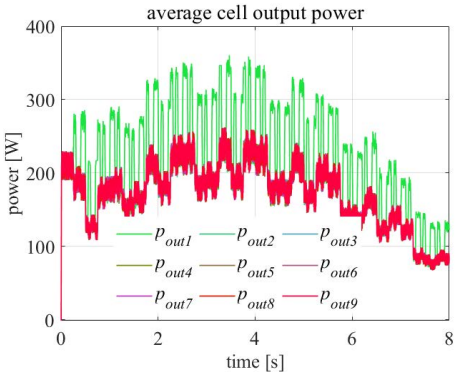

FIGURE 15. Average output power of the CHB power cells.

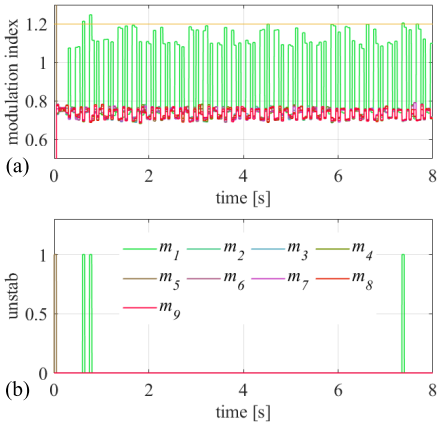

FIGURE 16. Modulation indexes (a), and stability flag (b).

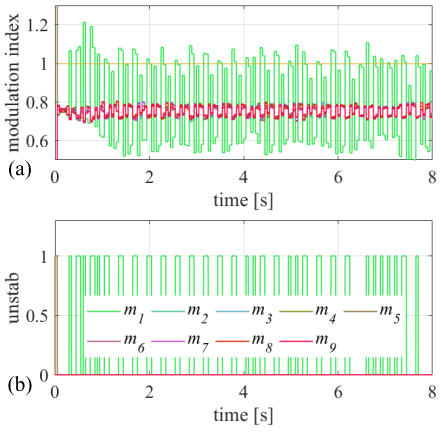

FIGURE 17. Modulation indexes (a), and stability flag (b) in the case of $m_{iUL} = 1$.

In our case, this limit cannot be reached because of the used modulation strategy which provides at least one cell in PWM mode, thus preventing the full square-wave operation.

The modulation indexes are reported in Fig. 16. It can be inferred that N-1 cells (i.e., 8 cells from #2 to #9) operate with their nominal modulation index, while the most powerful cell (i.e., cell#1) mainly operates in overmodulation region (i.e.,

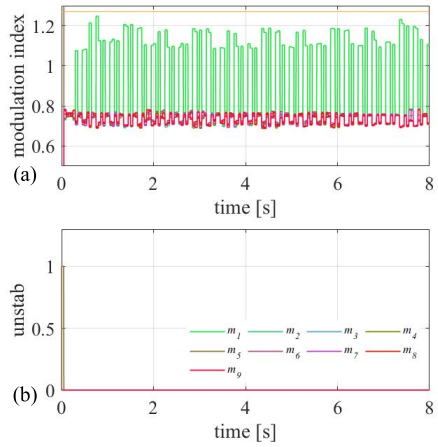

FIGURE 18. Modulation indexes (a), and stability flag (b) in the case of $m_{iUL} = 1.27$.

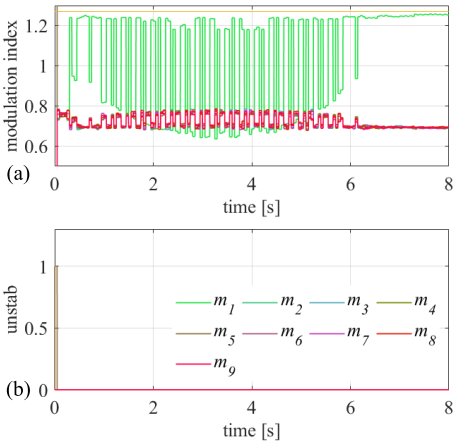

FIGURE 20. Modulation indexes (a), and stability flag (b) in the special case of mismatch and $m_{iUL} = 1.27$.

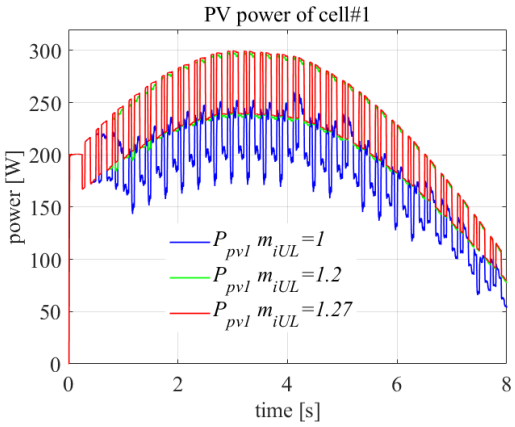

FIGURE 19. PV power of cell#1: upper limit of modulation index equal to 1 (blue line), to 1.2 (green line), to 1.27 (red line).

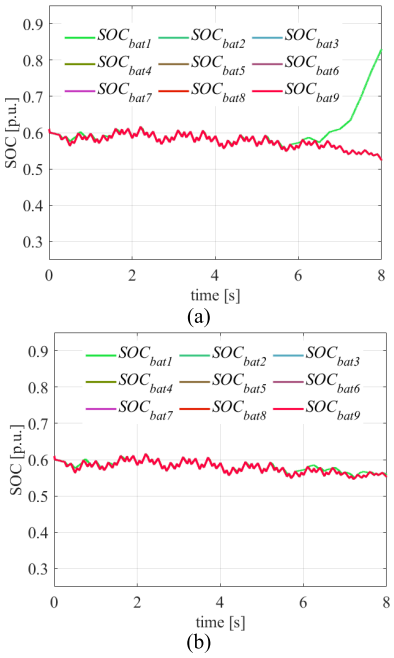

FIGURE 21. SOC versus time of the nine batteries: (a) $m_{iUL} = 1.27$; (b) $m_{iUL} = 1.2$.

in the time intervals in which a mismatch condition arises (see also Fig. 13).

Three times the upper limit of 1.2 is exceeded, but the control brings back the cell in the permitted range by stopping the MPPT, while increasing the PV reference voltage (until the modulation index comes back).

Now, it could be useful to understand what happens if the m_i upper limit is fixed to 1 or rather no overmodulation is allowed for the cell#1 (i.e., the most powerful) and also if the m_i upper limit is fixed to 1.27 (i.e., maximum value corresponding to square-wave operation).

In the former case, m_1 overcomes the limit many times, and it goes below the value of other cells, as can be seen in Fig. 17, while in the latter case (see Fig. 18) the upper limit of 1.27 is never reached (i.e., the modulation index control never acts).

This is reflected in the behavior of the average PV power of cell#1 (see Fig. 19). The value of $m_{iUL} = 1$ (i.e., no overmodulation is allowed for the most powerful cell) determines a strong reduction of power harvesting from PVG of cell#1, so limiting the overall power production. On the other hand, the behavior in case of $m_{iUL} = 1.2$ and $m_{iUL} = 1.27$ is similar, so being convinced the stability control is unnecessary.

With the aim of confuting this statement, it should be considered a special case, which will be analyzed in the following sub-section. Furthermore, it is worth noting that the circuit control is also able to obtain a good behavior in terms of output power quality.

C. SPECIAL CASE OF MISMATCH

N-1 cells (i.e., 8 cells from #2 to #9) are subjected to the irradiance profile shown in Fig. 6 in the time window 08÷16 (i.e., 8:00 AM÷4:00 PM), while cell#1 is subjected to a constant irradiance of 800 W/m^2. Two cases are considered:

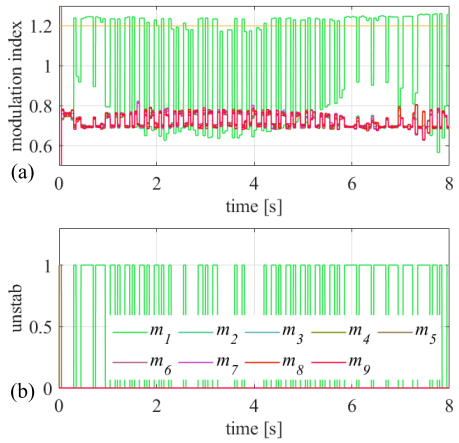

FIGURE 22. Modulation indexes (a), and stability flag (b) in the special case of mismatch and $m_{iUL} = 1.2$.

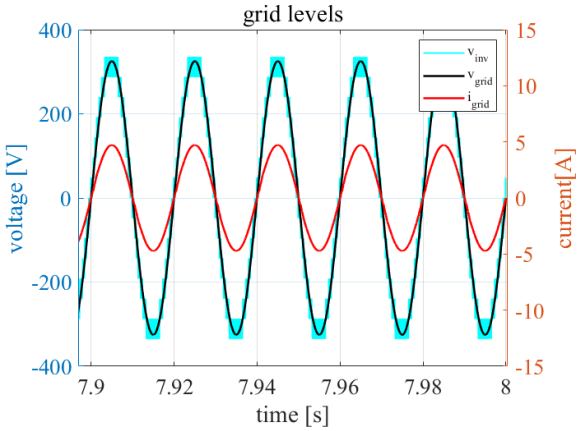

FIGURE 23. Behavior of grid current (red line), modulated voltage (cyan line), and the grid voltage (black line).

$m_{iUL} = 1.27$ and $m_{iUL} = 1.2$. In the first case the modulation index behavior is shown in Fig. 20.

As you can notice, the SOC of the cell#1 diverges from the desired behavior in the second part of the day when the mismatch between cell#1 and the others becomes deeper (see Fig. 21(a)). This deviation can be avoided by considering the second case under study with $m_{iUL} = 1.2$, whose modulation indexes are reported in Fig. 22.

The modulation index of cell#1 often overcomes the fixed upper limit of 1.2, thus causing the stability control action which has a beneficial effect on the SOC behavior.

In fact, Fig. 21(b) makes evident that the control is able to keep SOCs balanced as desired with no detrimental effect on the overall system performance.

The analysis of this special case highlights that by increasing the upper limit of the modulation index up to the theoretical maximum value of $4/\pi$, so extending the circuit operational boundaries, could not provide an enhanced result. This is because the effective maximum achievable value of modulation index upper limit depends on the used modulation technique.

At this point, it is necessary to observe that the proposed hybrid modulation strategy, presented in sub-section 3.B.2, entails a cell of the cascade, at least one per sorting cycle, to be in PWM mode, while the others can assume the remaining modes (i.e., 0 mode, ± 1 mode), thus the cells cannot reach a full square-wave operation ($m_{iUL} = 4/\pi$) [32]. As a consequence, the proper choice of the modulation index upper limit is relevant to obtain the desired behavior also in the case of deep mismatch conditions. Furthermore, as mentioned above, the overall system performance is not affected by the modulation index control as can be inferred from Fig. 23, where the grid behavior (voltage and current) along with the inverter output voltage (modulated voltage) is shown. The resulting power factor is practically unitary, while the grid current total harmonic distortion (THD) is of about 0.18% or rather well belove the limit of 5% fixed by the grid code.

V. CONCLUSION

This paper is mainly focused on the mitigation of the inherent power intermittency in PV CHB inverter by means of a distributed energy storage system whose SOC is kept balanced, thus ensuring a constant power delivery to the utility network.

This goal is achieved thanks to a suitable power scheduling method considering the average behavior of PV generation profile and the SOC error, so leading to a global power reference bringing the system to track on average the total available PV power. Then, the SOC error is also used to properly sort the cells in the cascade so that the proposed hybrid modulation scheme can keep individually balanced the SOCs in the structure. A complete set of simulated performance, both in uniform and mismatch conditions, proved the effectiveness of the proposed design and control. Moreover, a special case of study further highlighted the need of an adequate modulation index control to preserve the SOC balancing also in case of deep mismatch.

REFERENCES

[1] Publications. *IRENA International Renewable Energy Agency*. Accessed: Sep. 24, 2021. [Online]. Available: https://www.irena.org/

[2] C. A. Hill, M. C. Such, D. Chen, J. Gonzalez, and W. M. Grady, "Battery energy storage for enabling integration of distributed solar power generation," *IEEE Trans. Smart Grid*, vol. 3, no. 2, pp. 850–857, Jun. 2012.

[3] P. T. Krein and J. A. Galtieri, "Active management of photovoltaic system variability with power electronics," *IEEE J. Emerg. Sel. Topics Power Electron.*, vol. 9, no. 6, pp. 6507–6523, Dec. 2021.

[4] M. Salehi, M. Shahabadini, H. Iman-Eini, and M. Liserre, "Predictive control of grid-connected modified-CHB with reserve batteries in photovoltaic application under asymmetric operating condition," *IEEE Trans. Ind. Electron.*, vol. 69, no. 9, pp. 9019–9028, Sep. 2022.

[5] W. Liang, Y. Liu, and J. Peng, "A day and night operational quasi-Z source multilevel grid-tied PV power system to achieve active and reactive power control," *IEEE Trans. Power Electron.*, vol. 36, no. 1, pp. 474–492, Jan. 2021.

[6] W. Li and G. Joos, "Comparison of energy storage system technologies and configurations in a wind farm," in *Proc. IEEE Power Electron. Spec. Conf.*, Jun. 2007, pp. 1280–1285.

[7] M. Liserre, T. Sauter, and J. Y. Hung, "Future energy systems: Integrating renewable energy sources into the smart power grid through industrial electronics," *IEEE Ind. Electron. Mag.*, vol. 4, no. 1, pp. 18–37, Mar. 2010.

[8] M. Lei, Z. Yang, Y. Wang, H. Xu, L. Meng, J. C. Vasquez, and J. M. Guerrero, "Design of energy storage control strategy to improve the PV system power quality," in *Proc. IECON 42nd Annu. Conf. IEEE Ind. Electron. Soc.*, Oct. 2016, pp. 2022–2027.

[9] C.-Y. Tang, P.-T. Chen, and J.-H. Jheng, "Bidirectional power flow control and hybrid charging strategies for three-phase PV power and energy storage systems," *IEEE Trans. Power Electron.*, vol. 36, no. 11, pp. 12710–12720, Nov. 2021.

[10] S. Kumar, L. N. Patel, B. Singh, and A. L. Vyas, "Self-adjustable step-based control algorithm for grid-interactive multifunctional single-phase PV-battery system under abnormal grid conditions," *IEEE Trans. Ind. Appl.*, vol. 56, no. 3, pp. 2978–2987, May 2020.

[11] Y. Pan, A. Sangwongwanich, Y. Yang, X. Liu, M. Liserre, and F. Blaabjerg, "Flexible active power control of distributed photovoltaic systems with integrated battery using series converter configurations," *IEEE J. Emerg. Sel. Topics Power Electron.*, early access, Dec. 9, 2021, doi: 10.1109/JESTPE.2021.3134203.

[12] H. Beltran, I. Etxeberria-Otadui, E. Belenguer, and P. Rodriguez, "Power management strategies and energy storage needs to increase the operability of photovoltaic plants," *J. Renew. Sustain. Energy*, vol. 4, no. 6, Nov. 2012, Art. no. 063101.

[13] G. Brando, A. Dannier, I. Spina, and P. Tricoli, "Integrated BMS-MMC balancing technique highlighted by a novel space-vector based approach for BEVs application," *Energies*, vol. 10, no. 10, p. 1628, Oct. 2017.

[14] M. Vasiladiotis and A. Rufer, "Analysis and control of modular multilevel converters with integrated battery energy storage," *IEEE Trans. Power Electron.*, vol. 30, no. 1, pp. 163–175, Jan. 2015.

[15] M. A. Perez, S. Bernet, J. Rodriguez, S. Kouro, and R. Lizana, "Circuit topologies, modeling, control schemes, and applications of modular multilevel converters," *IEEE Trans. Power Electron.*, vol. 30, no. 1, pp. 4–17, Jan. 2015.

[16] Z. Wang, H. Lin, Y. Ma, X. Wang, T. Wang, and Z. Ze, "Analysis and control strategy of modular multilevel converter with integrated battery energy storages system based on voltage source mode," in *Proc. 20th Eur. Conf. Power Electron. Appl. (EPE ECCE Eur.)*, Sep. 2018, pp. P. 1–P.9.

[17] C. Sirico, R. Teodorescu, D. Séra, M. Coppola, P. Guerriero, D. Iannuzzi, and A. Dannier, "PV module-level CHB inverter with integrated battery energy storage system," *Energies*, vol. 12, no. 23, p. 4601, Dec. 2019.

[18] S. M. Goetz, C. Wang, Z. Li, D. L. K. Murphy, and A. V. Peterchev, "Concept of a distributed photovoltaic multilevel inverter with cascaded double H-bridge topology," *Int. J. Electr. Power Energy Syst.*, vol. 110, pp. 667–678, Sep. 2019.

[19] U. Sohail, H. Nademi, and L. E. Norum, "A reliable modular based PV-battery hybrid system with peak shaving capability," in *Proc. IEEE 19th Workshop Control Modeling Power Electron. (COMPEL)*, Jun. 2018, pp. 1–6.

[20] Q. Zhang and K. Sun, "A flexible power control for PV-battery hybrid system using cascaded H-bridge converters," *IEEE J. Emerg. Sel. Topics Power Electron.*, vol. 7, no. 4, pp. 2184–2195, Dec. 2019.

[21] L. Liu, H. Li, Z. Wu, and Y. Zhou, "A cascaded photovoltaic system integrating segmented energy storages with self-regulating power allocation control and wide range reactive power compensation," *IEEE Trans. Power Electron.*, vol. 26, no. 12, pp. 3545–3559, Dec. 2011.

[22] A. Marquez, J. I. Leon, S. Vazquez, L. G. Franquelo, and S. Kouro, "Operation of an hybrid PV-battery system with improved harmonic performance," in *Proc. IECON 43rd Annu. Conf. IEEE Ind. Electron. Soc.*, Oct. 2017, pp. 4272–4277.

[23] B. Ge, Y. Liu, H. Abu-Rub, and F. Z. Peng, "State-of-charge balancing control for a battery-energy-stored quasi-Z-source cascaded-multilevel-inverter-based photovoltaic power system," *IEEE Trans. Ind. Electron.*, vol. 65, no. 3, pp. 2268–2279, Mar. 2018.

[24] X. Li, D. Hui, and X. Lai, "Battery energy storage station (BESS)-based smoothing control of photovoltaic (PV) and wind power generation fluctuations," *IEEE Trans. Sustain. Energy*, vol. 4, no. 2, pp. 464–473, Apr. 2013.

[25] S. Stynski, W. Luo, A. Chub, L. G. Franquelo, M. Malinowski, and D. Vinnikov, "Utility-scale energy storage systems: Converters and control," *IEEE Ind. Electron. Mag.*, vol. 14, no. 4, pp. 32–52, Dec. 2020.

[26] V. Blahnik, T. Kosan, Z. Peroutka, and J. Talla, "Control of a single-phase cascaded H-bridge active rectifier under unbalanced load," *IEEE Trans. Power Electron.*, vol. 33, no. 6, pp. 5519–5527, Jun. 2018.

[27] M. Ciobotaru, R. Teodorescu, and F. Blaabjerg, "A new single-phase PLL structure based on second order generalized integrator," in *Proc. 37th IEEE Power Electron. Spec. Conf.*, Jun. 2006, pp. 1–6.

[28] D. N. Zmood and D. G. Holmes, "Stationary frame current regulation of PWM inverters with zero steady-state error," *IEEE Trans. Power Electron.*, vol. 18, no. 3, pp. 814–822, May 2003.

[29] R. Teodorescu, F. Blaabjerg, and M. Liserre, "Proportional-resonant controllers. A new breed of controllers suitable for grid-connected voltage-source converters," in *Proc. 9th Int. Conf. Optim. Elect. Electron. Equip. Optim*, 2004, pp. 9–14.

[30] EU Science Hub. *European Commission*. Accessed: Sep. 24, 2021. [Online]. Available: https://joint-research-centre.ec.europa.eu/pvgis-photovoltaic-geographical-information-system_en

[31] J.-M. Timmermans, A. Nikolian, J. De Hoog, R. Gopalakrishnan, S. Goutam, N. Omar, T. Coosemans, J. Van Mierlo, A. Warnecke, D. U. Sauer, M. Swierczynski, D. I. Stroe, E. Martinez-Laserna, E. Sarasketa-Zabala, J. Gastelurrutia, and N. Nerea, "Batteries 2020—Lithium-ion battery first and second life ageing, validated battery models, lifetime modelling and ageing assessment of thermal parameters," in *Proc. 18th Eur. Conf. Power Electron. Appl. (EPE ECCE Eur.)*, Sep. 2016, pp. 1–23.

[32] M. Coppola, P. Guerriero, D. Iannuzzi, S. Daliento, and A. D. Pizzo, "Extended operating range of PV module-level CHB inverter," *Int. J. Electr. Power Energy Syst.*, vol. 119, Jul. 2020, Art. no. 105892.

DIEGO IANNUZZI received the degree *(laude)* and Ph.D. degrees in electrical engineering from the University of Naples, in 1998 and 2001, respectively. He became an Associate Professor, in 2003. Since 2004, he has carried out research activity with the Traction Competence Centre of Campania. Since 2005, he has been an Associate Professor of electrical drives at the Faculty of Engineering, University of Naples Federico II. Since 2021, he has been a Full Professor of power electronics and electrical drives. He was a Founder Member of spin off, Power Naples Prototype Laboratory. He was a Founder Member of the IEEE International Conference on Electrical Systems for Aircraft, Railway, Ship Propulsions and Electrical Vehicles (ESARS-ITEC). He has 23 years of academic experience as a Researcher and a Professor in power electronics, electrical drives and machines. He is the Chief of the "Transportation Research Laboratory," DIETI. He has been engaged in the National and International Research Program supported by the European Community and the Italian Ministry of the University of Scientific Research. He is a Co-ordinator of the project ASPIRE, in the framework of EU-Program on Power Converters for Aircraft Smart Grid. He is also the Co-ordinator of international agreements between the University of Naples "Federico II" and Universities located in other parts of the world (e.g. the University of Texas at Dallas, the Institut Polytechnique de Tolouse, and Chiba University, Japan). He has contributed to 145 papers published worldwide in international journals and conferences. His research interests include the use of emerging technology, energy storage systems, and semiconductor devices applied to power converters and electrical drives in the sectors of traction drives (for road and railway vehicles) and renewable energy systems. His scientific activities are focused on the development of a modular multilevel converter (MMC) integrated with innovative energy storage devices (e.g. Lithium ion capacitors) for an ultrafast and wireless EV-charging station, integration of emerging energy storage systems in power electronic systems and electrification transportation field, energy management control of light railway vehicles, and SiC and GaN technology for electrical transportation. All of these activities are collaborations involving international partnerships with excellent research institutes and universities.

MARINO COPPOLA received the Laurea degree *(cum laude)* in electronic engineering and the Ph.D. degree in electronic and telecommunication engineering from the University of Napoli Federico II, Italy, in 2008 and 2012, respectively. From 2012 to 2015 and from 2019 to 2021, he has been a Postdoctoral Researcher at the Department of Electrical Engineering and Information Technologies, University of Napoli Federico II. From 2015 to 2018, he has been a Senior Researcher at the PNP Laboratory (a spin-off company of the University of Napoli Federico II). He is currently a Research Fellow at the Department of Electrical Engineering and Information Technologies, University of Napoli Federico II. He has been a Visiting Researcher at the Department of Energy Technology, Aalborg University, Denmark, and Laplace Laboratories, Institut National Polytechnique of Toulouse, France. He has coauthored 40 papers in refereed international journals and conference proceedings. His current research interests include design and control of power converters for photovoltaics and distributed power generation systems, integration of renewable energy resources in electrical systems, modulation of multilevel converters, design, and control of high efficiency dc–dc converters, and design of digital circuits on FPGA.

PIERLUIGI GUERRIERO (Member, IEEE) received the Laurea and Ph.D. degrees in electronic engineering from the University of Napoli Federico II, Naples, Italy, in 2007 and 2012, respectively.

He is currently working as an Assistant Professor with the Department of Electrical Engineering and Information Technology, University of Naples Federico II. He has coauthored more than 70 papers in refereed international journals and conference proceedings, and three patents. His research interests include modeling and characterization of solar cells, diagnostic and monitoring techniques for photovoltaic devices and systems, development of effective MPPT algorithms, as well as multilevel dc–ac converters for renewable energy applications.

ADOLFO DANNIER (Member, IEEE) received the degree and Ph.D. degrees in electrical engineering from the University Federico II of Naples, in 2003 and 2008, respectively, with a dissertation on multilevel converters with fault-tolerant structures. Since 2020, he has been an Associate Professor of converters, electrical machines and drives at the University of Naples Federico II and teaches ''modeling of electric machines and converters'' and ''power electronic converter.'' Active in the research topics of his scientific sector, he collaborated with national and international research projects, as attested by numerous and significant scientific publications. His research interests include high-performance dynamic drives with PM motors, conversion equipment, and electrical energy storage for electric vehicles and for the integration of renewable energy sources.

ANDREA DEL PIZZO (Member, IEEE) received the M.S. degree in electrical engineering from the University of Naples Federico II, in 1979.

He became an Assistant Professor with the University of Naples Federico II, in 1983, and a Full Professor of power electronics, electric machines and drives with the University of Naples Federico II, in 2001. He was also the President of the Electrical Engineering Faculty for many years. He is currently the Director of the Research Center of traction drives for air, road and marine propulsion. His main research interests include modeling and design of electrical machines and drives, powertrains with PM-brushless or induction motor drives for electrical propulsion of different types of vehicles, vector control motor drives, predictive control, and multi-modular converters. He was and is the scientific responsible of many research contracts with private companies and public institutions. He is involved in several scientific committees of international conferences, including as the general Chairperson.

Open Access funding provided by 'Università degli Studi di Genova' within the CRUI CARE Agreement